ADVANCED MATERIALS INTERFACES

www.advmatinterfaces.de

Alkali Metal Chlorides Based Hydrogel as Eco-Friendly Neutral Electrolyte for Bendable Solid-State Capacitor

Hu Li, Xinxin Wang, Wen Jiang, Haoyu Fu, Xiaoqiang Liang, Ke Zhang, Zhe Li, Chaochao Zhao, Hongqing Feng, Jia Nie, Ruping Liu, Gang Zhou, Yubo Fan, and Zhou Li**

Hydration greatly affects ionic state in an aqueous environment and thus influences their electrochemical performance. In this study, three alkali metal chlorides dissolved in neutral polyvinyl alcohol hydrogel are fully investigated for bendable solid-state TiO_2 nanotube capacitor (BSTC). Radius difference between bare ions and hydrated ions results in their obviously different electrochemical performance. Hydration makes lithium-ion (Li^+) possess the largest hydrated radius and the lowest mobility, which endows it the best capacitance performance in BSTC by electrochemical characterization. BSTC with hydrated Li^+ achieves high capacitance retention rates of 87% at 1 V for 3000 cycles and of 70% at 2 V for 2500 cycles. Additionally, it has no significant capacitance variation when stored for one month or bended to 120°.

1. Introduction

As energy storage device, electrochemical capacitors have attracted growing interest for the fast charge/discharge feature in recent years.[1] According to the mechanism of charge storage, electrochemical capacitors can be classified as electrical double layer capacitors (EDLCs) and pseudocapacitors. EDLCs are based on electrostatic charge diffusion and accumulation at the interface of electrode active material and electrolyte.[2] Pseudocapacitors are dominated by Faradaic reactions on electrode materials.[3] Acidic electrolytes (H_2SO_4, H_3PO_4) are usually used in electrochemical energy storage for their excellent conductivity, high ion concentration, and low equivalent resistance.[4] However, the acidic property endowed them with strong corrosion on metal current collector and metallic oxide. Additionally, the leakage of acid solution is harmful to environment and human health. For alkaline electrolytes,[5] KOH acted as the preferred candidate for carbon-based material and transition metallic oxide.[6] Whereas the alkaline electrolytes tend to cause electrolyte creepage, which made it difficult in packaging capacitor device.[7] Additionally, the operational voltage window of carbon materials is usually lower than 1 V due to their superior conductivity. Therefore, it is necessary to conduct further researches on solid-state capacitors with neutral electrolytes.

Alkali metal ions (Li^+, Na^+, and K^+) are commonly used as neutral electrolytes in last decades. Recently, neutral electrolytes with a wide operational voltage window (2.2 V) have been widely studied for their low price, easy availability, and environmental friendliness.[8] Alkali metal sulfates (Li_2SO_4, Na_2SO_4, and K_2SO_4) are usually utilized for liquid dielectric capacitor composed of carbon-based materials and transition metal oxides.[9] However, alkali sulfates are not suitable for solid-state capacitor due to their salting-out effects in polymer hydrogel.[10] Additionally, the alkali metal nitrates ($LiNO_3$, $NaNO_3$, and KNO_3) are not commonly used in capacitors for their poor cycling stability and low operation voltage.[11] In contrast, alkali metal chlorides showed excellent dissolubility and cycling stability in polyvinyl alcohol (PVA) hydrogel.[12] According to previous reports, the PVA–LiCl hydrogel contributed to structure stability of transition metal oxides (V_3O_7) in cycling test.[12b] The PVA–KCl hydrogel showed a good cycling stability (about 85% of capacitance retention for 5000 cycles at 0.8 V) in conductive metal–organic framework.[12c] These two researches mainly focus on the capacitive performance of electrode material and showed low operation voltages of 1[12b] and 0.8 V.[12c]

H. Li, Dr. X. X. Wang, Dr. W. Jiang, Dr. H. Fu, X. Liang, K. Zhang, Z. Li, C. Zhao, Dr. H. Feng, Prof. Z. Li
Beijing Institute of Nanoenergy and Nanosystems
Chinese Academy of Sciences
Beijing 100083, China
E-mail: zli@binn.cas.cn

H. Li, Prof. G. Zhou, Prof. Y. Fan
Key laboratory for biomechanics and Mechanobiology of Ministry of Education
School of Biological Science and Medical Engineering
Beihang University
Beijing 100083, China
E-mail: yubofan@buaa.edu.cn

H. Li, Prof. G. Zhou, Prof. Y. Fan
Beijing Advanced Innovation Centre for Biomedical Engineering
Beihang University
Beijing 100191, China

Dr. X. X. Wang, X. Liang, Dr. H. Feng, Prof. Z. Li
CAS Center for Excellence in Nanoscience
Beijing Institute of Nanoenergy and Nanosystems
Chinese Academy of Sciences
Beijing 100083, China

J. Nie, Prof. R. Liu
Beijing Institute of Graphic Communication
Beijing 102600, China

The ORCID identification number(s) for the author(s) of this article can be found under https://doi.org/10.1002/admi.201701648.

DOI: 10.1002/admi.201701648

In last decades, active material structures and components of capacitors were extensively studied,[2–4,13] few comprehensive researches were conducted about neutral electrolytes in solid-state capacitors with alkali metal chlorides.

Herein, we conducted a full research about alkali metal chlorides as neutral electrolytes in solid-state capacitors. The highly ordered porous titanium dioxide (TiO_2) nanotubes were used as active material, which offered an extremely large, solvated ion accessible surface area.[14] PVA hydrogel integrated the separator and the electrolytes into a single layer, which prevented leakage and electrical contact between electrodes. It also avoided potential leakage for the bounded electrolytes within the polymer matrix.[15,16] The neutral property of these electrolytes makes them eco-friendly to our environment and human health. The charge storage mechanism was discussed for the capacitive difference in three alkali metal chlorides. Hydration endows the bare Li^+ with the largest hydrated radius and lowest migration rate, the low migration rate contributed to the capacitive performance and made the hydrated Li^+ obtain the largest capacitance. This research provided the optimal electrolyte candidate from these alkali metal chlorides for neutral solid-state EDLCs. The superior performance of hydrated Li^+ proved its great application potential in bendable, eco-friendly, and durable energy storage device.

2. Results and Discussion

2.1. Mechanism Analysis of Solid-State BSTC

As illustrated in **Figure 1**a, BSTC possessed a symmetric sandwich structure, Ti foil and TiO_2 nanotube layer served as current collector and active material, respectively. Alkali metal chlorides were dissolved in PVA matrix as hydrogel electrolyte. Ions were randomly distributed in PVA matrix hydrogel without an external electric field (upper, Figure 1b). Cations and anions in hydrogel will migrate to the interfaces of TiO_2 nanotubes and electrolyte under electrostatic interaction (bottom, Figure 1b). To enhance the mechanical stability and electrical conductivity of TiO_2 nanotubes and Ti foils, the as-prepared samples were post-treated at 400 °C for 2 h in Ar gas atmosphere according to previous reports (Figure 1c).[14b,17] The temperature of 400 °C is a superior annealing parameter, which can make TiO_2 nanotubes effectively transform from amorphous phase to anatase phase and improve the capacitance of TiO_2 nanotubes. A lower temperature can only inadequately change the crystal phase. A higher temperature will transform anatase phase to rutile phase and destroy the structure of TiO_2 nanotube array, which is negative for energy storage.[17] As shown in Figure 1d, no peaks of anatase phase (○) appeared in the red curve, and only reflection peaks (□) appeared from Ti foil in the red curve. It indicates that the untreated TiO_2 nanotubes are amorphous. After thermal annealing at 400 °C strong peak signals of anatase phase appeared in the black curve. It proved that the amorphous phase of TiO_2 nanotube transformed to anatase phase successfully.

2.2. Surface Morphology Characterization of TiO_2 Nanotubes

Detailed morphologies of TiO_2 nanotube arrays were shown in **Figure 2**. The as-prepared TiO_2 nanotube layer consisted of nanotube arrays with a porous nanostructure (Figure 2a), and the inner diameter ranges around 100 nm (Figure 2b). The open-end nanotube structure offers an extremely large, solvated ion accessible surface area for charge accumulation.

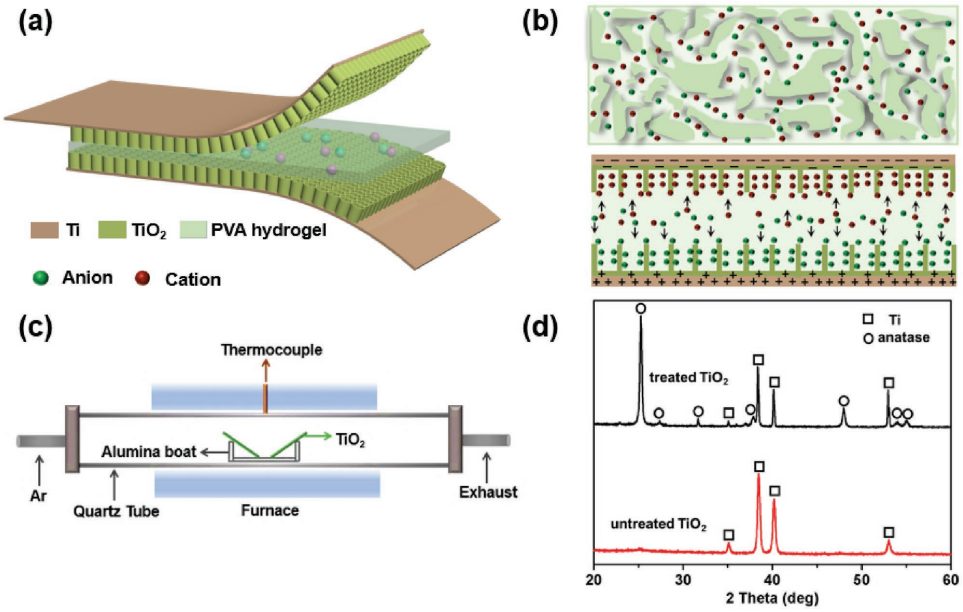

Figure 1. a) Structure diagram of BSTC. b) Schematic in initial state (upper) and charged state (bottom) of alkali metal chlorides–PVA neutral hydrogel electrolytes. c) Thermal annealing of TiO_2 nanotubes in Ar gas atmosphere. d) XRD patterns collected from untreated TiO_2 and thermal-treated TiO_2 nanotubes. The squares (□) in black and red curves represent Ti signals reflected from Ti foil. The circles (○) in black curve represent anatase phase signals from TiO_2 crystal phase.

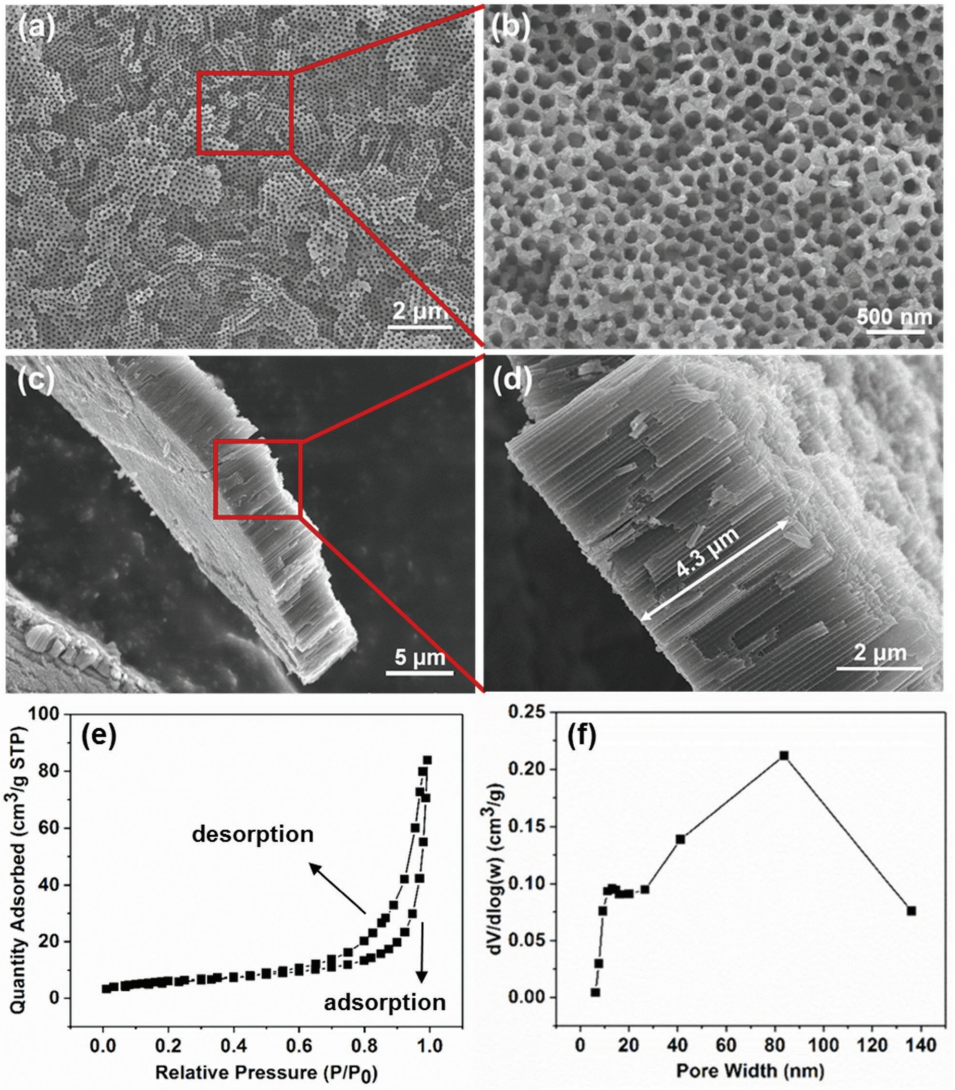

Figure 2. SEM images of the as-prepared TiO_2 nanostructures grown on Ti foil. a,b) Top view and enlarged morphologies of TiO_2 nanotubes, respectively. c,d) Cross-sectional view and enlarged morphologies of TiO_2 nanotube layer. e,f) BET adsorption–desorption and BJH pore size analysis profiles of TiO_2 nanotube.

Additionally, it possesses a flat bottom and tightly aligned structures between nanotubes (Figure 2c). The unique structure of TiO_2 nanotube layer on Ti foil contributes to the high electron conduction between nanotube arrays and the Ti foil as well as the short ion diffusion path through walls of nanotubes. The thickness of nanotube layer is about 4.3 μm (Figure 2d), the thin property of TiO_2 nanotube layer conduces to keeping the structural stability during the actual bending process.

The surface area and porosity of TiO_2 nanotube layer were measured with adsorption–desorption experiment using Brunauer–Emmett–Teller (BET) and Barrett–Joyner–Halenda (BJH) method (Figure 2e,f). The adsorption–desorption profile indicated that the TiO_2 nanotube has a type of *IV* isotherm, suggesting the nanoporous nature of TiO_2 nanotube layer. The BJH adsorption average pore width was 61.55 nm. The average pore volume was 0.204 $cm^3\ g^{-1}$. The BET surface area of TiO_2 nanotube was estimated to be 21.73 $m^2\ g^{-1}$, which provided a very large, solvated ion accessible surface area for charge accumulation.

2.3. Ionic State of Alkali Metal Cations and Anions in PVA Hydrogel

Ionic states in solution are easily influenced by a liquid environment and greatly affect the electrochemical performance of capacitor.[8,18] Water molecules in PVA hydrogel possessed an asymmetrical configuration with the hydrogen atoms attached at about 104° to each other. This special configuration generated a slightly polarized water molecule.[18] The molecular polarity leads to alignment of water molecules around the ions to form hydration shells, which in turn alter the physical dimension of ions. Positively charged ions (Li^+, Na^+, and K^+) attract the negative ends (i.e., oxygen) of the polarized water molecules

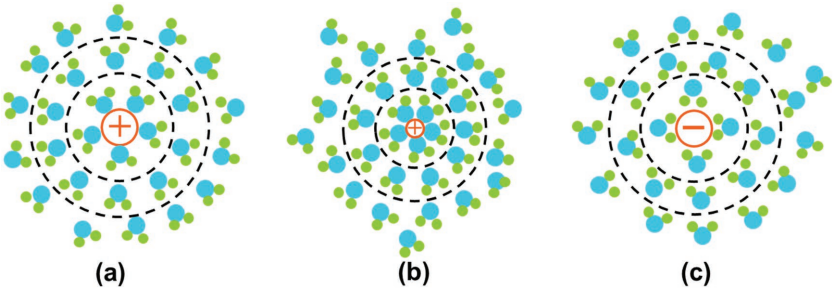

Figure 3. Schematic diagram illustrating hydration shells around a) a large monovalent cation, b) a small monovalent cation, and c) a large monovalent anion. Inner and outer circles denote the primary and secondary hydration shells, respectively. Water molecule (H_2O); Hydrogen (H); Oxygen (O).

and negatively charged ions (Cl^-) attract the positive ends (i.e., hydrogen).[18a] The hydration process greatly influence the radii and even change the size order of free ions. Here, three alkali metal chlorides (LiCl, NaCl, and KCl) have the same anion (Cl^-) in this research, therefore, only difference of cations (Li^+, Na^+, and K^+) were discussed below.

As shown in **Figure 3**, this schematic diagram illustrated hydration shells around monovalent ions. The water molecules within the primary shell are somewhat ordered through hydrogel bonding. The order degree decreases from primary shell to secondary shell to the outermost shell for the decreasing electrostatic force. The smaller bare ionic radius, the stronger absorption of water molecules around the ions, which means that the smaller monovalent ions can bond more water molecules tightly. Charges and crystal radius together determine the hydrated radius.[18] Certainly, it is impossible to precisely measure the number of water molecules around cations and anions because the aqueous solution is a dynamic system and the numbers can easily change. All the number values of water molecules around cations and anions in **Table 1** are average numbers. According to the data in Table 1, bare ion radii of Li^+, Na^+, and K^+ increase as follows: $Li^+ < Na^+ < K^+$. However, hydrated Li^+ bonded the most average water molecules (i.e., 22), which endowed Li^+ the largest hydrated radius (0.382 nm). Hydrated radii of Li^+, Na^+, and K^+ decrease as follows: $Li^+ > Na^+ > K^+$. Compared with hydrated Na+ and K+, the largest ion radius of hydrated Li^+ leads to the least mobility and the lowest diffusion ability in PVA hydrogel bulk. The poor mobility and low diffusion contribute to keeping hydrated Li^+ remain near to the interface of TiO_2 nanotube and electrolyte during discharging and then quickly appear at this interface during charging, which is conducive to ion storage.[8]

Table 1. Bare and hydrated radii[18d,e] and hydration numbers[18b] of ions.

Ions	Li^+	Na^+	K^+	Cl^-
Bare ion radii [nm]	0.094	0.117	0.149	0.164
Hydrated radii [nm]	0.382	0.358	0.331	0.332
Hydration numbers	22	13	7	5

2.4. CV Performance of Three Alkali Metal Chlorides

To investigate the electrochemical performance of three alkali metal chlorides, BSTC was assembled for cyclic voltammetry (CV) measurement at different scan rates. To ensure the sufficient contact and infiltration between the as-prepared PVA hydrogel and nanotube layer, the morphologies from cross-section of TiO_2 nanotube layer before and after addition of PVA hydrogel were characterized in Figure S1 in the Supporting Information. The scanning electron microscope (SEM) images shows that PVA hydrogel infiltrated into TiO_2 nanotube layer and covered its surface successfully. The energy dispersive X-ray (EDX) spectrum and mapping (Figures S2 and S3, Supporting Information) gave the relevant elements on nanotube surface. These two characterizations showed that the alkali chlorides were also infiltrated into nanotube layer successfully. These results indicated the sufficient contact between charges and nanotubes in charging and discharging process, which ensured the accuracy of following electrochemical test.

The CV curves showed that the best charge propagation correlated with capacitance was obtained for LiCl from 10 to 100 mV s^{-1} (**Figure 4**a–c). The measured current values were recalculated to mF cm^{-2} according to the following formula[19]

$$C_a = \frac{\int I\,dV}{\nu \cdot \Delta V \cdot S} \quad (1)$$

where C_a (mF cm^{-2}) is the areal capacitance, I (A) is the response current, ν (V s^{-1}) is the potential scan rate, ΔV (V) is the potential window and S (cm^2) is the effective surface area of BSTC.

The best charge propagation and capacitance values were achieved for LiCl. This result is in strict connection with the mobility of hydrated alkali metal ions, which increases in the following order: $Li^+ < Na^+ < K^+$. Different from pseudocapacitors, in which redox process requires fast migration of ions into the interface of electrode and electrolyte, EDLCs just rely on simple charging and discharging of the electrical double layers and does not need very high ion mobility.[18] When the porous structure of TiO_2 nanotubes was saturated by hydrated ions, the hydrated ions (Li^+, Na^+, K^+, and Cl^-) already located on the interface of TiO_2 nanotube and electrolyte are attracted and pushed off from TiO_2 nanotube on a small distance under the external electric field. Herein, we assume that the high mobility of hydrated ions might aggravate their fast and efficient charge propagation in PVA hydrogel, it makes the hydrated ions keep far away from the interface of TiO_2 nanotube and electrolyte in discharging, which in turn makes them difficult to return back in charging. It will weaken the capacitance of hydrated ions. The results obtained from three alkali metal chlorides in Figure 4 clearly proved the assumption. No matter at a slow scan rate (10 mV s^{-1}) or a fast scan rate (100 mV s^{-1}), the capacitance value is the highest for LiCl when compared with NaCl and KCl (Figure 4d).

Capacitance decrement rate of LiCl from 10 mV s^{-1} (5.3 mF cm^{-2}) to 100 mV s^{-1} (3.3 mF cm^{-2}) is about 37.7%.

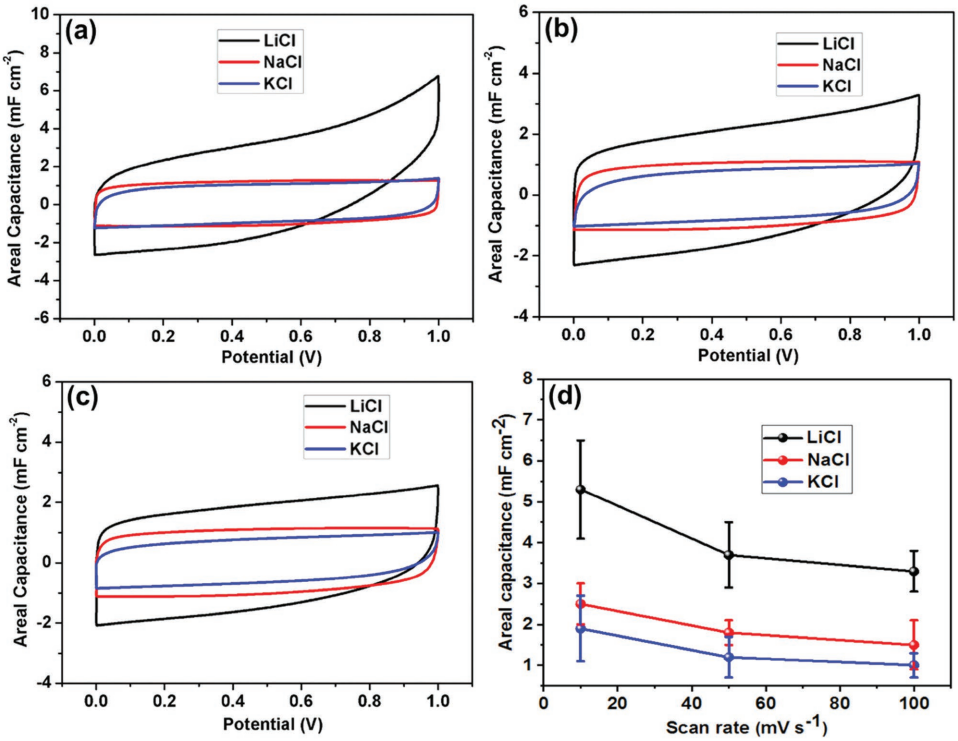

Figure 4. CV measurement of three alkali metal chlorides at different scan rates. a) 10 mV s^{-1}, b) 50 mV s^{-1}, and c) 100 mV s^{-1}. d) Capacitance versus scan rate for different alkali metal chlorides. All the concentrations of alkali metal chlorides in PVA hydrogel were 1 mol L^{-1}. Error bars represent the standard deviation.

However, capacitance decrement rates of NaCl and LiCl are 40 and 47.4%, respectively. That is to say, the capacitance decrement rate increase in sequence: LiCl < NaCl < KCl. It indicates that the numbers of detained hydrated Na^+ and K^+ in PVA hydrogel are larger than that of hydrated Li^+. It also proved that the high mobility of hydrated Na^+ and K^+ aggravated the fast and efficient charge migration in PVA hydrogel in discharging, which make it difficult for them return back in charging. Hydrated Li^+ has the largest hydrated radius, which make it easy to stay near to the interface of TiO_2 nanotube and electrolyte and appear in the interface quickly in charging and discharging. This feature leads to the difference in three alkali metal chloride electrolytes and endows LiCl the best CV performance.

2.5. Galvanostatic Charge/Discharge (GCD) Performance

To further investigate electrochemical performance of three alkali metal chlorides and verify the assumption above, a GCD technique was applied at current density in range between 0.06 and 0.2 mA cm^{-2} (**Figure 5**a–c). The symmetric triangular shape of GCD curves demonstrated the excellent faradaic capacitive charge storage, which was in good agreement with the CV results. The discharge time increases successively from KCl to LiCl at the same current density. The discharge areal capacitance can be estimated by the following equation[18a,b]

$$C_a = \frac{2 \cdot I \cdot \Delta t}{\Delta V \cdot S} \tag{2}$$

where C_a (mF cm^{-2}) is the areal capacitance, I (A) is the charge/discharge current, Δt (s) is the discharge time, ΔV (V) is the potential window, and S (cm^2) is the effective surface area of BSTC. According to Equation (2), LiCl showed the best capacitance performance, which was consistent with the results in Figure 4. As shown in Figure 5d, GCD technique strictly proved the same tendency in Figure 4 d. LiCl showed the highest capacitance in the current density range from 0.06 to 2 mA cm^{-2}. Capacitance decrement rates of LiCl, NaCl, and KCl were 23.5, 30.4, and 33.3%, respectively. This result was in good accordance with that in CV characterization in Figure 4d and also proved the assumption above. Alkali metal ions (Li^+, Na^+, and K^+) are strongly solvated in water and turned into hydrated ions. Monovalent Li^+ bonded the most average numbers of water molecules (i.e., 22) and possessed the largest hydrated ion radius (i.e., 0.382 nm). It endows hydrated Li^+ the lowest mobility and diffusion ability in PVA hydrogel. As discussed above, they rather remain near to the interface of TiO_2 nanotube and electrolytes during discharging process and quickly appear at the interface during charging. By contrast, Na^+ and K^+ can only bond 13 and 7 water molecules, respectively. The hydrated Na^+ and K^+ with smaller hydrated radii possessed higher mobility and diffusion ability, therefore, they can migrate into PVA hydrogel for a long distance during discharging and their return to the interface of TiO_2 nanotube and

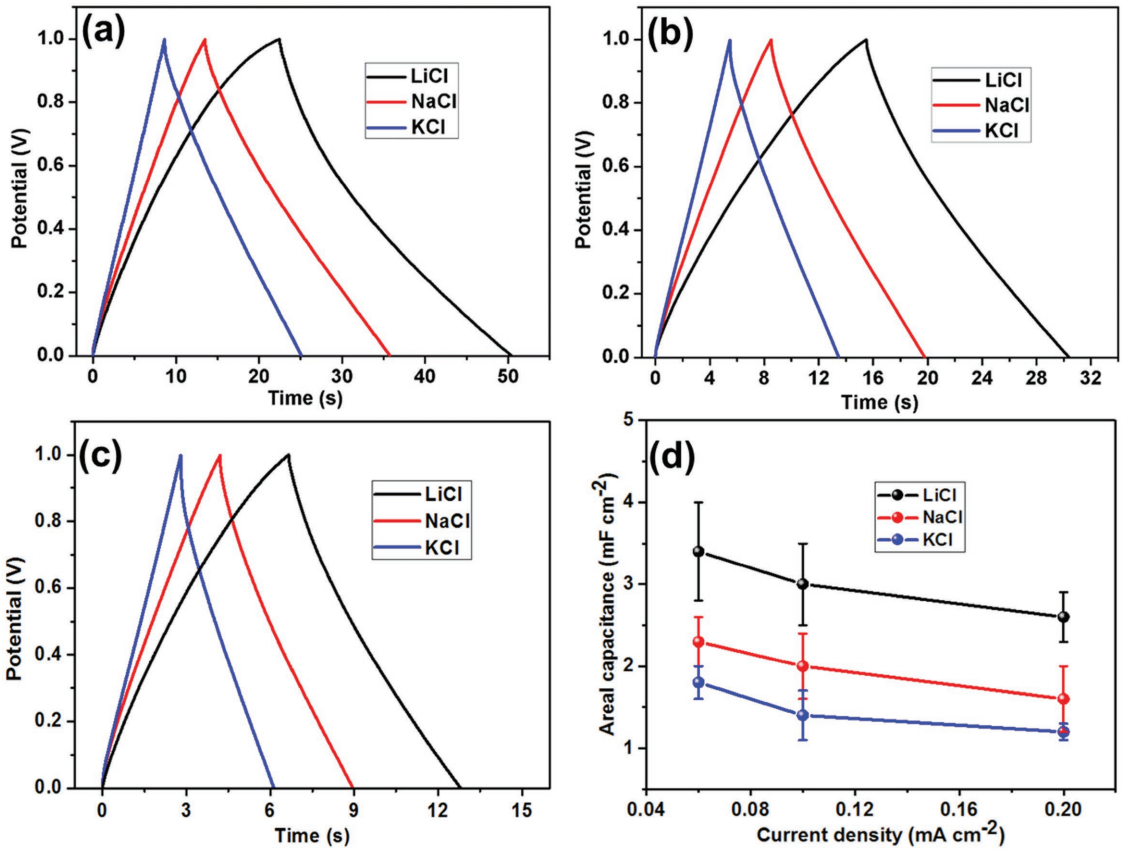

Figure 5. Galvanostatic charge/discharge curves collected at different current density. a) 0.06 mA cm^{-2}, b) 0.1 mA cm^{-2}, and c) 0.2 mA cm^{-2} for three alkali metal chlorides. d) Capacitance versus current density for three alkali metal chlorides. All the concentrations of three alkali metal chlorides in PVA hydrogel were 1 mol L^{-1}. Error bars represent the standard deviation.

electrolyte is not so fast. Therefore, the capacitive performance of NaCl and KCl is inferior to that of LiCl.

2.6. Electrochemical Impedance Spectroscopy (EIS) Measurement

EIS measurement was carried out in three alkali metal chlorides electrolytes in the frequency range between 10 mHz and 100 kHz. In the complex plane, the real component, Z (Re), shows the Ohmic property and the imaginary component, $-Z$ (Im), shows the capacitive property. The theoretical Nyquist plot of a capacitor contains three parts that are relevant on the frequencies in theory. At the very high frequency, the capacitor behaves like a pure resistor. At the low frequency, the imaginary component sharply increases until it resembles a vertical line, indicating the capacitive property. At the medium frequency, it can reflect the influence of electrode porosity on capacitive property. When it decreases from the very high frequency, the signals penetrate into the porous nanotube deeper and deeper, then more and more nanotube surfaces become available for hydrated ion adsorption. The medium frequency region is in connection with the electrolyte penetration in porous structure. This region is commonly called the Warburg curve.[20]

Figure 6a shows the EIS spectrum of BSTC in three alkali metal chlorides. All the EIS curves show a linear trend in the low frequency region, an arc shaped curve or a similar arc shaped curve in the high frequency region. The Warburg curves are known as the straight line at a 45° angle from the lower left region to the upper right region in EIS spectrum in Figure 6a. The Warburg curve of LiCl is shorter than those of NaCl and KCl, indicating a more effective propagation of hydrated Li^+ to the TiO_2 nanotube surface. The equivalent series resistance of three alkali metal chlorides are obtained from the intercept of real axis (Z (Re)) (Figure 6b). At the highest frequency (i.e., 100 kHz), BSTC with LiCl was characterized by the smallest impedance value of 6 Ω. The NaCl showed a medium impedance value of 10 Ω. The KCl showed the largest impedance value of 15 Ω. It directly proves that the current in LiCl electrolyte can pass through TiO_2 nanotube/PVA hydrogel/TiO_2 nanotube more easily than NaCl and KCl, and the hydrated Li^+ cations can form double electrode layer very quickly on the interface of TiO_2 nanotube and PVA hydrogel in charging. This feature is mainly attributable to the poor mobility of hydrated Li^+ cations, which make hydrated Li^+ cations stay near to the interface and return back quickly in charging.

As shown in Figure 6c, capacitance of BSTC was recalculated from the imaginary part of the complex impedance by[21]

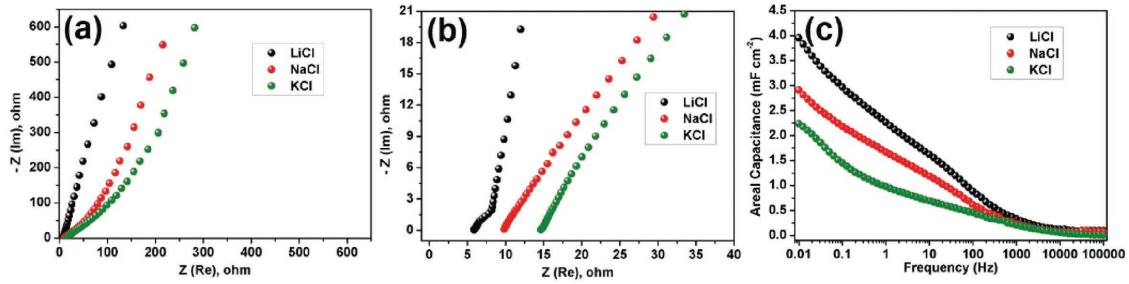

Figure 6. Nyquist plots of BSTCs operated in a) a full range of frequencies, b) a high-frequency region, and c) capacitance versus frequency dependence. All the concentrations of alkali metal chlorides were kept at 1 mol L^{-1}.

$$C_a = \frac{-1}{\pi f \cdot Z_{im} \cdot S} \tag{3}$$

where f (Hz) is the frequency, Z_{im} is the imaginary part of the electrode resistance, S (cm^2) is the effective surface area of BSTC. It also proved the best charge propagation of LiCl electrolyte. BSTC with LiCl electrolyte showed the highest capacitance value at the low frequency range of 100 Hz to10 mHz. Additionally, the decrement rate of capacitance increase from LiCl to KCl at the frequency range from 0.1 to 10 Hz. It proved that the mobility decreases from hydrated Li^+ cations to hydrated K^+ cations. The poor mobility of hydrated Li^+ cations contributes to charge propagation near to the interface of TiO_2 nanotube and PVA hydrogel. All the results obtained by EIS agreed well with the other characterization above.

2.7. Voltage Window and Cycle Stability of LiCl Electrolyte

All the measurement above proved that LiCl was the best candidate in energy storage among three alkali metal chlorides. To prove the application potential of LiCl for solid-state capacitor, it is necessary to explore the operation voltage window and cycle stability of BSTC with LiCl electrolyte. As shown in **Figure 7**, CV measurement and cycle stability characterization were conducted below 2.7 V. CV curves below 2.5 V are close to rectangular shape and no significant current increase appeared until 2.7 V. The rapid current increase at 2.7 V implied the decomposition of hydrogen or chlorine evolution. In other words, BSTC with LiCl electrolyte can keep capacitive performance stable using operation voltage blow 2.5 V. As shown in Figure 7b, the capacitance values of BSTC at 1 V decreased slowly in the first

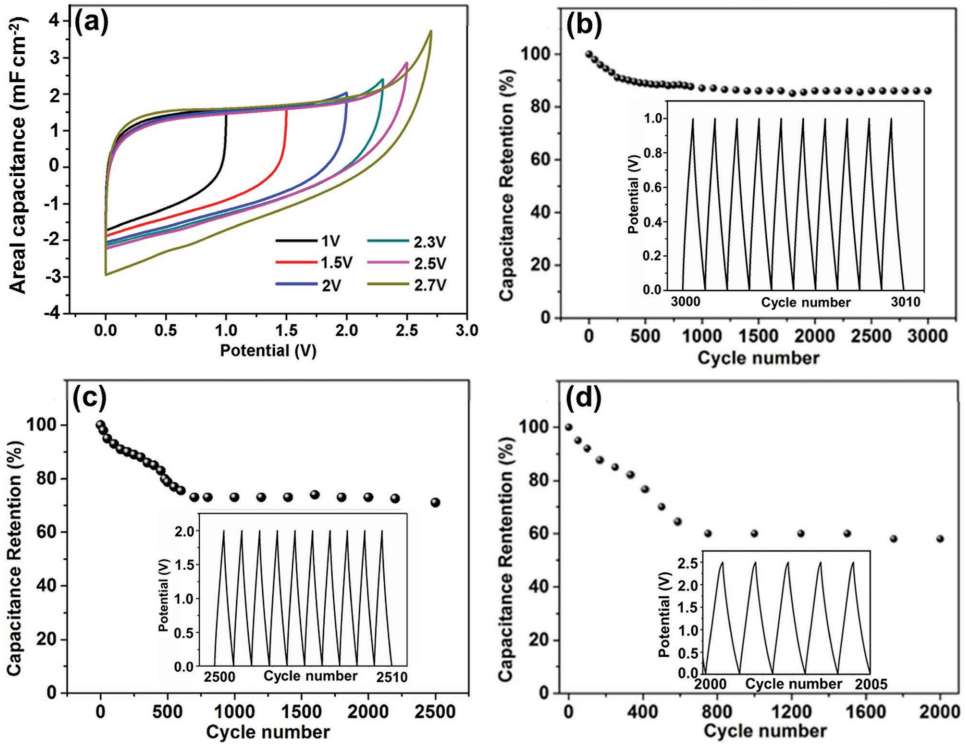

Figure 7. a) CV curves of BSTC in different operational voltage windows. b–d) Cycling performance at the operation voltages of 1, 2, and 2.5 V, respectively. All the measurement were conducted with LiCl electrolyte at 1 mol L^{-1}. The insets show the GCD curves after (b) 3000 cycles, (c) 2500 cycles, and (d) 2000 cycles, respectively.

300 cycles, after that the capacitance values reached a smooth plateau. Remarkably, about 87% of the initial capacitance was retained after 3000 cycles. The capacitor can still maintain normal work and keep a good charge–discharge behavior after 3000 cycles (inset in Figure 7b). As shown in Figure 7c, a higher operation voltage (2 V) induced a reduction in capacitance in the first 500 cycles, and then it remained stable for further cycling. An outstanding capacitance retention of 70% was achieved after 2500 cycles. It can also keep a good working performance after 2500 cycles (inset in Figure 7c). However, the operation voltage of 2.5 V induced a rapid decrease in capacitance in the first 700 cycles, then a poor capacitance retention of 58% was achieved after 2000 cycles (Figure 7d). Although it kept a good charge–discharge behavior after 2000 cycles (inset in Figure 7d), it is not suitable for energy storage due to the inferior capacitance performance. The surface morphology of TiO_2 nanotube layer kept its structural integrity at 1 and 2 V after thousands of cycles. The edges of TiO_2 nanotubes changed a little at 2.5 V, it may attribute to the high operation voltage, and some of the nanotube edges were broken in the cycling process (Figure S4, Supporting Information). Briefly, it is reasonable to apply an operation voltage of 2 V as the safe voltage window for energy storage in practical application.

Table 2. Summary and comparison of capacitive performance with previous researches on transition metal oxides and conductive polymers for EDLCs.

Ref.	Electrode materials	Electrolyte	Operation voltage	Capacitance retention	Cycle number
[14a]	H-TiO_2 nanotube	0.5 M Na_2SO_4 aqueous	0.8 V	96.9%	10 000
[14a]	Untreated TiO_2 nanotube	0.5 M Na_2SO_4 Aqueous	0.8 V	65.2%	10 000
[14a]	air-TiO_2 nanotube	0.5 M Na_2SO_4 aqueous	0.8 V	55.7%	10 000
[22]	V_2O_5 nanoporous network	0.5 M K_2SO_4 aqueous	1 V	76%	600
[23]	V_2O_5-PPy microsphere	5 M $LiNO_3$ aqueous	1 V	70%	100
[23]	Bare V_2O_5	5 M $LiNO_3$ aqueous	1 V	43%	100
[24]	Bare PANI	2 M H_2SO_4 aqueous	1 V	40%	1000
[24]	PANI-carbon sphere	2 M H_2SO_4 aqueous	1 V	73%	1000
[25]	Bare MnO_2	1 M Na_2SO_4 aqueous	1 V	69%	1000
[25]	GO-MnO_2	1 M Na_2SO_4 aqueous	1 V	84.1%	1000
[26]	Fe_3O_4 nanoparticle	1 M Na_2SO_3 aqueous	1 V	73%	2000
[27]	MnO_2 nanotube	1 M Na_2SO_4 aqueous	1 V	81%	2000
[28]	PPy-gel	1.5 w/w H_3PO_4/PVA solid-state	0.8 V	83.6%	2000
[29]	Mesoporous α-MnO_2	1 M Na_2SO_4 aqueous	1 V	90%	8000
[30]	TiO_2-PANI nanowire	1 M H_2SO_4 aqueous	0.8 V	97.2%	10 000
[31]	MnO_2@Co/C nanoplatelet	1 M Na_2SO_4 aqueous	0.8 V	89.1%	10 000
Our work	Ar-TiO_2 nanotube	1 M PVA/alkali metal chlorides solid-state	1 V	87%	3000
			2 V	70%	2500
			2.5 V	58%	2000

2.8. Performance Comparison with Previous Researches

To prove the outstanding application potential of BSTC with LiCl electrolyte, we compared the cycle stability and operation voltage of BSTC with previous researches on bare transition metal oxides (V_2O_5, MnO_2, Fe_3O_4), bare conductive polymer (PANI, PPy), and their composites with carbon materials (GO-MnO_2, PANI-carbon sphere,) for EDLCs. Performance of materials above in pseudocapacitors were not discussed here. As shown in **Table 2** and **Figure 8**, most of the operational voltage windows focus on 0.8 and 1 V. Most of the bare active materials (bare V_2O_5, bare MnO_2, MnO_2 nanotube, Fe_3O_4 nanoparticle, PANI; 1 V) have a low cycle stability less than 3000 cycles. The composite active materials of TiO_2-PANI (1 M H_2SO_4) and MnO_2 nanoplatelet@Co/C (1 M Na_2SO_4) have a superior cycle stability up to 10 000 cycles, which are suitable for commercial application. However, the acidic electrolyte (H_2SO_4) and alkali metal sulfates (Na_2SO_4) are not suitable for solid-state transition metal oxide capacitor for their acidic property or salting-out effects in polymer matrix. Additionally, these supercapacitors are usually operated under a low voltage window (0.8 V), which make them inconvenient for use in high voltage applications. Here, in our work, the bare TiO_2 nanotube annealed in argon (Ar-TiO_2) can achieve about 87% of capacitance retention at 1 V after 3000 cycles and 70% of capacitance retention at 2 V after 2500 cycles with solid-state LiCl–PVA hydrogel electrolyte. In general, BSTC with LiCl electrolyte in PVA hydrogel achieved a superior cycle performance with a high operation voltage window of 2 V, and it proved the practical application potential of BSTC in energy storage to some extent. In the future, the bare TiO_2 nanotube has the potential to be modified with other materials to achieve a higher cycle numbers with high capacitance retention at 2 V.

2.9. Mechanical Property and Stability of Solid-State BSTC with LiCl Electrolyte

The storage stability and flexibility of solid-state BSTC with LiCl electrolyte was further investigated to demonstrate its superior performance in practical application. **Figure 9**a shows the CV curves of BSTC measured as it was prepared, stored for one week and for one month, respectively. Little variation formed in the shape and area of CV curves, which indicates a good electrochemical stability and endurable stability of BSTC with LiCl electrolyte in PVA hydrogel. Figure 9b presents the CV curves of BSTC bent at different degrees. The CV performance remained nearly unchanged at different bending curvatures of 30°, 90°, and 120°. Capacitance increased slightly as the bend angle varied from 0° to 30°. Such improvement is probably resulted from the decrease in distance of positive and negative electrodes. All the results indicated the excellent stability and flexibility of solid-state BSTC with LiCl electrolyte in PVA hydrogel electrolyte.

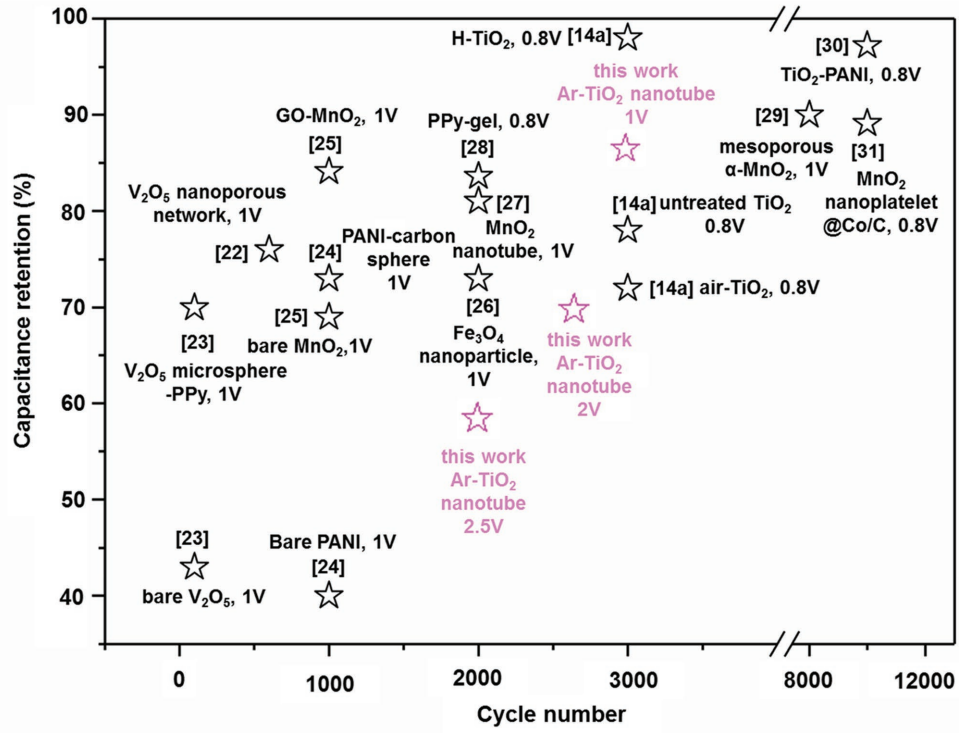

Figure 8. Summary and comparison of capacitive performance with previous researches on transition metal oxides and conductive polymers for EDLCs.

2.10. Practical Application of Solid-State BSTC with LiCl Electrolyte

To demonstrate the practical application of solid-state BSTC with LiCl electrolyte, two as-fabricated BSTCs were assembled in series (**Figure 10**a) and in parallel (Figure 10b). Compared with a single BSTC with an operation voltage of 2 V, the two BSTCs connected in series exhibited a charge/discharge voltage window of 4 V with similar charge/discharge time (38 s in Figure 10a), which indicated good maintenance in capacitive performance of a single BSTC. The discharge time of the parallel connected BSTCs is about two times that of a single BSTC at the same current density (Figure 10b). When the tandem BSTCs were charged to 4 V and kept stable for 20 s (Figure 10c), a green light-emitting diode (LED) (working voltage: 3.2 V) was lighted up (Figure 10d). These results demonstrated that BSTCs with LiCl–PVA hydrogel have a great potential in practical application as energy-storage devices.

3. Conclusion

In summary, based on the porous TiO_2 nanotubes, alkali metal chlorides in neutral PVA hydrogel were fully investigated for BSTC. The ionic state of cations and anions were discussed basing on the hydration mechanism. Hydration effect transformed bare alkali metal ions into hydrated ions, changing the radii of alkali metal ions as follows: $Li^+ > Na^+ > K^+$. Hydrated Li^+

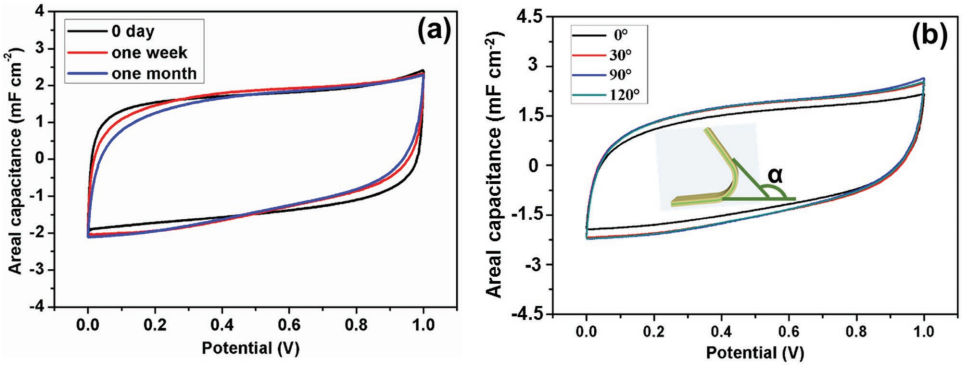

Figure 9. a) CV curves of BSTC stored for different durations of time. b) Mechanical property of BSTC under various bending degrees. Scan rate: 200 mV s^{-1}. The inset explicates the bending mode of BSTC.

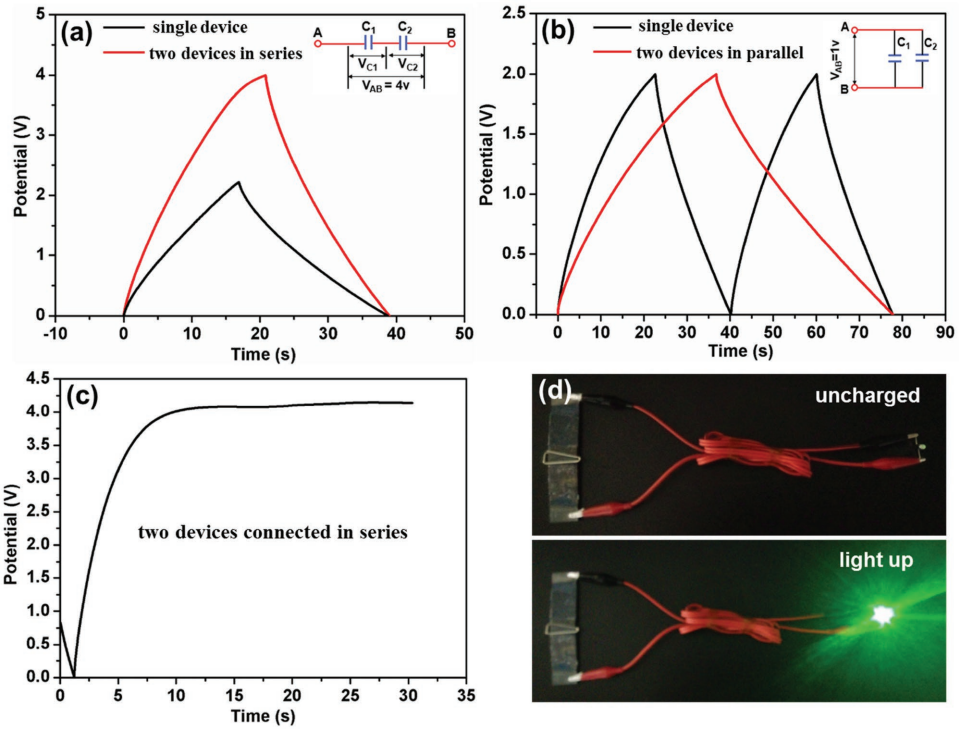

Figure 10. GCD curves of a single BSTC and two BSTCs connected a) in series and b) in parallel. c) Galvanostatic charge curve of two BSTCs connected in series at a current density of 0.2 mA cm^{-2}. d) Photograph of a green LED powered by two BSTCs connected in series. The insets explicate connection circuit diagrams of BSTCs.

cations have the largest radius, resulting in their poor mobility in PVA hydrogel. This feature contributes to retaining hydrated Li^+ near to the interface of TiO_2 nanotubes and PVA hydrogel and returning back to the interface very quickly in charging, which make LiCl show the best capacitive performance in three alkali metal chlorides. The LiCl electrolyte for solid-state BSTC possessed a high operation voltage window of 2 V and superior capacitance retention rates of 70% after 2500 cycles at 2 V and 87% after 3000 cycles at 1 V. Additionally, the LiCl electrolyte in PVA hydrogel for BSTC has no significant capacitance variation when stored for one month or bent to 120°. All characterization prove that LiCl is the best candidate in three alkali metal chlorides for solid-state capacitor. The superior performance of LiCl electrolyte in PVA hydrogel also proved its great application potential in bendable, eco-friendly, and durable energy storage device.

4. Experimental Section

Preparation of TiO_2 Nanotubes: TiO_2 nanotubes were synthesized by electrochemical anodic oxidation.[32] Prior to the electrochemical anodic oxidation, Ti foil (size: 2 cm × 4 cm; thickness, 0.1 mm) was cleaned by ultrasonication in acetone, ethanol, and deionized (DI) water successively. Then the Ti foil was anodized at a constant voltage of 50 V for 3 h at room temperature, with Ti foil as working electrode and a graphite plate (size: 6 cm × 6 cm) as cathode in an ethylene glycol aqueous solution (quantity ratio: 89.5 wt% ethylene glycol; 10 wt% DI water) containing 0.5 wt% NH_4F. The actual Ti foil area in the solution above was 2 cm × 2.5 cm. The prepared reaction solution above were only used for two Ti foils each time, then replaced with newly prepared reaction solution. The graphite plate was cleaned with DI water and ethyl alcohol at the end of every anodic oxidation process. The as-prepared TiO_2 nanotubes were thoroughly washed with ethanol and DI water, and then blow-dried with pure N_2. Then the TiO_2 nanotubes were placed in the middle position of the tube furnace and annealed in Ar (argon) atmosphere at 400 °C for 2 h.[14b,17] The heating rate of the tube furnace (BEQ, BTF-1200C, An Hui BEQ Equipment Technology CO., Ltd) was 2 °C min^{-1}, after keeping a constant temperature (400 °C) for 2 h, the furnace was cooled naturally. The gas flow velocity was maintained at 100 sccm throughout the annealing process.

Preparation of Alkali Metal Chloride–PVA Gel: The PVA powder (2 g) was dissolved in DI water (20 mL) by sonication at 80 °C. After the PVA was completely dissolved, the alkali metal chloride (LiCl, NaCl, or KCl) (20 mmol) was added into the PVA hydrogel under vigorous stirring until it formed into a homogeneous sticky solution. Then the solution was cooled down to room temperature and became a clear and transparent hydrogel.

Material Characterization and Electrochemical Measurement: The morphologies of TiO_2 nanotubes were characterized by SEM (HITACHI, SU8020). The composition of the samples were investigated via X-ray diffraction (XRD, PANalytical, X'Pert^3 Powder) with Cu Kα radiation (λ = 1.5418 Å). The surface area and porosity of TiO_2 nanotube were measured with adsorption–desorption experiment using BET and BJH method (micromeritics, Surface Area and Porosity Analyzer, ASAP 2020 HD88).

To ensure a fully infiltration of electrolytes into TiO_2 nanotube layer, the Ti foil with TiO_2 nanotubes was immersed into the 1 M alkali metal chloride aqueous solution without PVA for 24 h before the assembly of BSTC device. Then two pieces of the as-prepared Ti foils were immersed into the as-prepared PVA hydrogel electrolyte for 12 h, and then press them together in air for 2 h. The infiltration of electrolytes and PVA hydrogel was verified by EDX (IXRF SYSTEMS, Model 550i) analysis.

The electrochemical properties of the as-fabricated BSTCs were investigated in a two-electrode configuration using electrochemical workstation (CHI660E) and impedance/gain-phase analyzer (solartron, SI1260) at room temperature. The effective contact area of BSTC was 2 cm × 2.5 cm. The contact area was used in calculating the areal capacitance of BSTC.

Supporting Information

Supporting Information is available from the Wiley Online Library or from the author.

Acknowledgements

H.L. and X.X.W. contributed equally in this work. This work was supported by the national key R&D project from Minister of Science and Technology, China (Grant no. 2016YFA0202703), NSFC (Grant nos. 31571006, 81601629, 61501039), Beijing Talents Fund (Grant no. 2015000021223ZK21), the Beijing Natural Science Foundation (Grant nos. 2182091, 2162017) and "Thousands Talents" program for pioneer researcher and his innovation team.

Conflict of Interest

The authors declare no conflict of interest.

Keywords

alkali metal chlorides, hydrated radius, neutral hydrogels, solid-state capacitors, TiO_2 nanotubes

Received: December 16, 2017
Revised: February 11, 2018
Published online:

[1] a) B. Duong, Z. N. Yu, P. Gangopadhyay, S. Seraphin, N. Peyghambarian, J. Thomas, *Adv. Mater. Interfaces* **2014**, *1*, 1300014; b) P. Du, H. C. Liu, C. Yi, K. Wang, X. Gong, *ACS Appl. Mater. Interfaces* **2015**, *7*, 23932; c) Z. Yu, L. Tetard, L. Zhai, J. Thomas, *Energy Environ. Sci.* **2015**, *8*, 702.

[2] X. He, C. P. Yang, G. L. Zhang, D. W. Shi, Q. A. Huang, H. B. Xiao, Y. Liu, R. Xiong, *Mater. Des.* **2016**, *106*, 74.

[3] Y. Hu, J. Wang, X. H. Jiang, Y. F. Zheng, Z. X. Chen, *Appl. Surf. Sci.* **2013**, *271*, 193.

[4] a) C. F. Zhang, T. M. Higgins, S. H. Park, S. E. O'Brien, D. H. Long, J. N. Coleman, V. Nicolosi, *Nano Energy* **2016**, *28*, 495; b) D. Zhang, Y. Wu, T. Li, Y. Huang, A. Zhang, M. Miao, *ACS Appl. Mater. Interfaces* **2015**, *7*, 25835; c) G. G. Jang, B. Song, L. Y. Li, J. K. Keum, Y. D. Jiang, A. Hunt, K. S. Moon, C. P. Wong, M. Z. Hu, *Nano Energy* **2017**, *32*, 88.

[5] a) X. Cai, S. H. Lim, C. K. Poh, L. Lai, J. Lin, Z. Shen, *J. Power Sources* **2015**, *275*, 298; b) Y. G. Wang, L. Cheng, Y. Y. Xia, *J. Power Sources* **2006**, *153*, 191; c) S. Y. Kim, H. M. Jeong, J. H. Kwon, I. W. Ock, W. H. Suh, G. D. Stucky, J. K. Kang, *Energy Environ. Sci.* **2015**, *8*, 188.

[6] a) E. Raymundo-Piñero, M. Cadek, F. Béguin, *Adv. Funct. Mater.* **2009**, *19*, 1032; b) Y. Xiao, S. Liu, F. Li, A. Zhang, J. Zhao, S. Fang, D. Jia, *Adv. Funct. Mater.* **2012**, *22*, 4052; c) J. N. Recka, R. Cortez, S. Xie, M. Zhang, M. O'Keefe, F. Dogan, *Appl. Surf. Sci.* **2012**, *258*, 5599.

[7] S. Nohara, H. Wada, N. Furukawa, H. Inoue, M. Morita, C. Iwakura, *Electrochim. Acta* **2003**, *48*, 749.

[8] K. Fic, G. Lota, M. Meller, E. Frackowiak, *Energy Environ. Sci.* **2012**, *5*, 5842.

[9] a) Y. K. Hsu, Y. C. Chen, Y. G. Lin, L. C. Chen, K. H. Chen, *J. Mater. Chem.* **2012**, *22*, 3383; b) M. Sawangphruk, P. Srimuk, P. Chiochan, A. Krittayavathananon, S. Luanwuthi, J. Limtrakul, *Carbon* **2013**, *60*, 109; c) H. Li, H. Ouyang, M. Yu, N. Wu, X. X. Wang, W. Jiang, Z. Liu, J. J. Tian, Y. M. Jin, H. Q. Feng, Y. B. Fan, Z. Li, *Small* **2017**, *13*, 1603642; d) Z. Hu, X. Xiao, C. Chen, T. Q. Li, L. Huang, C. F. Zhang, J. Su, L. Miao, J. J. Jiang, Y. R. Zhang, J. Zhou, *Nano Energy* **2015**, *11*, 226; e) L. Athouël, F. Moser, R. Dugas, O. Crosnier, D. Bélanger, T. Brousse, *J. Phys. Chem. C* **2008**, *112*, 7270; f) J. Gomez, E. E. Kalu, *J. Power Sources* **2013**, *230*, 218.

[10] M. J. Hey, D. P. Jackson, H. Yan, *Polymer* **2005**, *46*, 2567.

[11] L. M. Chen, Q. Y. Lai, Y. J. Hao, Y. Zhao, X. Y. Ji, *J. Alloys Compd.* **2009**, *467*, 465.

[12] a) H. Muta, M. Miwa, M. Satoh. *Polymer* **2001**, *42*, 6313; b) G. M. Wang, X. H. Lu, Y. C. Ling, T. Zhai, H. Y. Wang, Y. X. Tong, Y. Li. *ACS Nano* **2012**, *6*, 10296; c) W. H. Li, K. Ding, H. R. Tian, M. S. Yao, B. Nath, W. H. Deng, Y. B. Wang, G. Xu. *Adv. Mater.* **2017**, *27*, 1702067.

[13] a) P. Tammela, Z. H. Wang, S. Frykstrand, P. Zhang, I. M. Sintorn, L. Nyholm, M. Strømme, *RSC Adv.* **2015**, *5*, 16405; b) T. Qian, C. F. Yu, S. S. Wu, J. Shen, *J. Mater. Chem. A* **2013**, *1*, 6539.

[14] a) X. H. Lu, G. M. Wang, T. Zhai, M. H. Yu, J. Y. Gan, Y. X. Tong, Y. Li, *Nano Lett.* **2012**, *12*, 1690; b) J. J. Qiu, F. W. Zhuge, K. Lou, X. M. Li, X. D. Gao, X. Y. Gan, W. D. Yu, H. K. Kim, Y. H. Hwang, *J. Mater. Chem.* **2011**, *21*, 5062.

[15] M. Kaempgen, C. K. Chan, J. Ma, Y. Cui, G. Gruner, *Nano Lett.* **2009**, *9*, 1872.

[16] a) N. A. Choudhury, S. Sampath, A. K. Shukla. *Energy Environ. Sci.* **2009**, *2*, 55; b) C. Zhong, Y. D. Deng, W. B. Hu, J. L. Qiao, L. Zhang, J. J. Zhang. *Chem. Soc. Rev.* **2015**, *44*, 7484.

[17] a) K. Zhu, N. R. Neale, A. F. Halverson, J. Y. Kim, A. J. Frank, *J. Phys. Chem. C* **2010**, *114*, 13433; b) O. K. Varghese, D. Gong, M. Paulose, C. A. Grimes, E. C. Dickey, *J. Mater. Res.* **2003**, *18*, 156.

[18] a) B. Tansel, J. Sager, T. Rector, J. Garland, R. F. Strayer, L. Levine, M. Roberts, M. Hummerick, J. Bauer, *Sep. Sci. Technol.* **2006**, *51*, 40; b) A. J. Rutgers, Y. Hendrikx, *Trans. Faraday Soc.* **1962**, *58*, 2184; c) M. Y. Kiriukhin, K. D. Collins, *Biophys. Chem.* **2002**, *99*, 155; d) E. R. Nightingale Jr., *J. Phys. Chem.* **1959**, *63*, 1381; e) A. G. Volkov, S. Paula, D. W. Deamer, *Bioelectrochem. Bioenerg.* **1997**, *42*, 153.

[19] Y. X. Xu, Z. Y. Lin, X. Q. Huang, Y. Liu, Y. Huang, X. F. Duan, *ACS Nano* **2013**, *7*, 4042.

[20] C. Portet, P. L. Taberna, P. Simon, C. Laberty-Robert, *Electrochim. Acta* **2004**, *49*, 905.

[21] a) R. Kumar, R. Kant, *Electrochim. Acta* **2016**, *95*, 275; b) M. D. Levi, M. R. Lukatskaya, S. Sigalov, M. Beidaghi, N. Shpigel, L. Daikhin, D. Aurbach, M. W. Barsoum, Y. Gogotsi, *Adv. Energy Mater.* **2015**, *5*, 1400815; c) Y. R. Nian, H. Teng, *J. Electroanal. Chem.* **2003**, *540*, 119.

[22] B. Saravanakumar, K. K. Purushothaman, G. Muralidharan, *ACS Appl. Mater. Interfaces* **2012**, *4*, 4484.

[23] J. Yang, T. B. Lan, J. D. Liu, Y. F. Song, M. D. Wei, *Electrochim. Acta* **2013**, *105*, 489.

[24] Z. Lei, Z. Chen, X. S. Zhao, *J. Phys. Chem. C* **2010**, *114*, 19867.

[25] S. Chen, J. Zhu, X. Wu, Q. Han, *ACS Nano* **2010**, *4*, 2822.

[26] L. Wang, H. Ji, S. Wang, L. Kong, X. Jiang, G. Yang, *Nanoscale* **2013**, *5*, 3793.

[27] H. Xia, J. K. Feng, H. L. Wang, M. O. Lai, L. Lu, *J. Power Sources* **2010**, *195*, 4410.

[28] C. Zhao, C. Y. Wang, Z. L. Yue, K. W. Shu, G. G. Wallace, *ACS Appl. Mater. Interfaces* **2013**, *5*, 9008.

[29] S. Bag, C. R. Raj, *J. Mater. Chem. A* **2016**, *4*, 587.

[30] P. Zhang, Z. M. Liu, Y. P. Liu, H. B. Fan, Y. Q. Jiao, B. M. Chen, *Electrochim. Acta* **2015**, *184*, 1.

[31] J. Zhi, O. Reiser, F. Q. Huang, *ACS Appl. Mater. Interfaces* **2016**, *8*, 8452.

[32] a) S. P. Albu, A. Ghicov, J. M. Macak, R. Hahn, P. Schmuki. *Nano Lett.* **2007**, *7*, 1286; b) P. Roy, S. Berger, P. Schmuki. *Angew. Chem., Int. Ed.* **2011**, *50*, 2904.